This article has been accepted for publication in a future issue of this journal, but has not been fully edited. Content may change prior to final publication. Citation information: DOI 10.1109/JESTPE.2015.2448633, IEEE Journal of Emerging and Selected Topics in Power Electronics

A Maximum Power Tracking Technique for Grid-Connected DFIG-Based Wind Turbines

Fariba Fateh, *Student Member, IEEE*, Warren N. White, and Don Gruenbacher, *Member, IEEE*

***Abstract* — In this paper, a maximum power tracking technique is presented for doubly fed induction generator (DFIG)-based wind turbines. The presented technique is a novel version of the conventional method, i.e. the electrical torque is proportional to the square of the rotor speed, in which the proportional-coefficient is adaptively adjusted in real-time through three control laws. The first control law calculates the desired electrical torque using feedback linearization, assuming that the power capture coefficient and the desired rotor speed are instantaneously identified. The second control law estimates real-time values of the power capture coefficient from a Lyapunov-based analysis, and the third control law provides the desired rotor speed. These control laws cause the turbine to adaptively adjust the rotor speed towards a desired speed in which the operating point moves in the direction of increasing the power capture coefficient. The proposed maximum power tracking method differs distinctly from the perturb-and-observe scheme by eliminating a need for adding a dither or perturbation signal, and robustly tracks the trajectory of maximum power points even in the event of a sudden wind speed change that can cause the perturb-and-observe technique to fail. In this paper, the NREL 5 MW reference wind turbine model is used to demonstrate the validity and robustness of the proposed method.**

***Index Terms* — Wind turbines, DFIG based wind turbines, nonlinear control, maximum power tracking.**

I. Introduction

Various control schemes for maximum power seeking in wind turbines have been presented in the literature [1]-[17]. Many are based on different nonlinear control strategies that can generally be categorized into the conventional control law [1]-[3], perturb-and-observe [4], hill-climbing [5] and hybrid techniques [6]-[17] in which, for example, the step size in a hill-climbing method is updated using fuzzy logic or neural network algorithms. In the conventional technique, the electrical torque is proportional to the square of the rotor speed while the controller gain needs to adaptively be adjusted in real-time. The perturb-and-observe and hill-climbing techniques may fail in seeking the maximum power in case of a rapid wind speed change [16]. The significance of the technique presented herein is that the rotor speed can adaptively be tracked through power coefficient estimation, even in the event of a sudden wind speed change. Herein, the presented method requires neither a perturbation nor a dither signal to track the trajectory of maximum power points.

Manuscript received January 14, 2015; revised May 2, 2015; May 28, 2015; accepted June 4, 2015.

Copyright (c) 2015 IEEE. Personal use of this material is permitted. However, permission to use this material for any other purposes must be obtained from the IEEE by sending a request to pubs-permissions@ieee.org.

F. Fateh and D. Gruenbacher are with the Department of Electrical and Computer Engineering, Kansas State University, Manhattan, KS 66506 USA (e-mail: fateh@ksu.edu; grue@ksu.edu).

W. White is with the Department of Mechanical and Nuclear Engineering, Kansas State University, Manhattan, KS 66506 USA (e-mail: wnw@ksu.edu).

To verify the validity of presented maximum power seeking technique, a full-order model of the electrical and mechanical subsystems of a DFIG-based wind turbine is implemented in this work. The electrical subsystem includes a doubly fed induction generator, back-to-back converters connected between the rotor and stator circuits, and a transmission line between the stator circuit and the grid. The mechanical subsystem consists of the blade aerodynamics and the drivetrain dynamics. The mechanical subsystem is modeled using the FAST (Fatigue, Aerodynamics, Structures, and Turbulence) simulator, which has been developed by the National Renewal Energy Laboratory (NREL) [18], which has been used as the analysis tool to examine the validity of the control schemes applied to wind turbines in the literature [10],[13],[14].

This paper is organized as follows. In Section II, a survey of maximum power seeking techniques for wind turbines is presented. In Section III, the aerodynamics of wind turbines are reviewed for the sake of continuity of the discussion. In Section IV, formulas and simulation models for subsystems of a DFIG-based wind turbine are given. In Section V, the proposed control laws are described in detail. In Section VI, simulation results are demonstrated in two different wind scenarios to confirm the validity and robustness of the developed control scheme, using the NREL 5MW wind turbine model. Furthermore, in Section VII, the proposed maximum power seeking scheme is studied in three subsections; (*i*) sensitivity of the maximum power seeking method with respect to variations of two main control parameters is investigated, (*ii*) seamless transition between low- and high-wind speed regions is demonstrated, and (*iii*) the conventional technique, in which the electrical torque is proportional to the square of the rotor speed, is used as a benchmark to investigate the dynamic behavior of the proposed control scheme. Finally, a summary of findings is provided as the conclusion section.

II. Review of Maximum Power Seeking Techniques

In this section, some of the maximum power seeking techniques for wind turbines are briefly reviewed [1]-[17]. In the conventional control law, which is described by Leithead et al. in [1], and Johnson et al. in [2] and [3], the desired electric torque is set to be proportional to the square of the rotor speed, i.e. $k\omega_R^2$. The square-law can best be understood from wind turbine power curves for different wind speeds, see Fig. 1. As can be seen, the trajectory of the maximum power falls in a $k\omega_R^3$ curve as the wind speed varies. This means the drivetrain torque must move on a $k\omega_R^2$ curve. However, for a wide range of wind speed variation, the challenge is to adaptively adjust the controller gain, k [10]. Moreover, the maximum power trajectory moves with changes in

2168-6777 (c) 2015 IEEE. Personal use is permitted, but republication/redistribution requires IEEE permission. See http://www.ieee.org/publications_standards/publications/rights/index.html for more information.

This article has been accepted for publication in a future issue of this journal, but has not been fully edited. Content may change prior to final publication. Citation information: DOI 10.1109/JESTPE.2015.2448633, IEEE Journal of Emerging and Selected Topics in Power Electronics

environmental parameters, e.g. air-density [2]. Thus, a lookup table method, artificial intelligence algorithms, or adaptive control schemes might be implemented in conjunction with the square-law to find real-time optimum value of the controller gain.

The perturb-and-observe method, presented by Hawkins et al. in [4], uses the sign of the gradient of the turbine captured power with respect to the rotor speed due to a perturbation added in the control signal. This technique can be sensitive to noise and perturbation size, particularly close to the power curve peak. Similarly, Ghaffari et al. [5] presented a maximum seeking algorithm using a sinusoidal dither signal added to the reference (command) rotor speed to estimate the gradient of the output power with respect to the rotor speed. The dither signal frequency must be low and its amplitude should be sufficiently small compared to the rotor speed [5]. In these techniques, one major problem that can lead to failure of the tracking process is the lack of distinction between the power differences resulting from the change in the wind with that resulting from a power change due to adding a perturbation [16].

Fuzzy logic and neural network algorithms have also been used to reduce the uncertainties faced by the aforementioned maximum power seeking in wind turbines [6]-[9]. Two of those methods are briefly reviewed in the following. Simoes et al. in [6] applied a fuzzy logic controller superimposed upon the hill-climbing concept. In this technique, the fuzzy controller updates the value of rotor speed change, $\Delta\omega_R$, in each hill-climbing step to track the maximum output power. While the technique is a non-model-based method and insensitive to noisy signals, a rule-base table and membership functions are required as the prior knowledge. Hui Li et al. in [8] presented a technique based on the optimum tip-speed ratio as a known feature for a wind turbine. Therefore, the wind speed is estimated using a neural network algorithm. In this scheme, the input signals are the measured power and rotor speed, and the output will be the desired rotor speed. Moreover, another neural network scheme is used to compensate the potential drift of the wind turbine power coefficient due to environmental variations. This is performed through utilizing a pseudo-power curve.

Adaptive control schemes have also been used to improve the maximum power capture methods [10]-[15]. Two of those methods are briefly reviewed in the following. Iyasere et al. in [10] presented a nonlinear control (electrical) torque that simultaneously minimizes the errors between measured and desired values of blade pitch angle and rotor speed while the maximum power capture coefficient is considered as a known parameter for a wind turbine. The desired values of rotor speed and blade pitch angle are also updated in real-time, when the first and second derivatives of the desired variables are bounded. In this technique the wind speed is assumed to be constant or slowly time varying. Beltran, et al. in [14] presented a hybrid technique where a second order sliding mode controller is combined with the conventional square-law torque control. In this technique, the mechanical (or aerodynamic) torque is estimated using a second order sliding mode observer, and an error is defined as the difference between the estimated torque and optimum torque values.

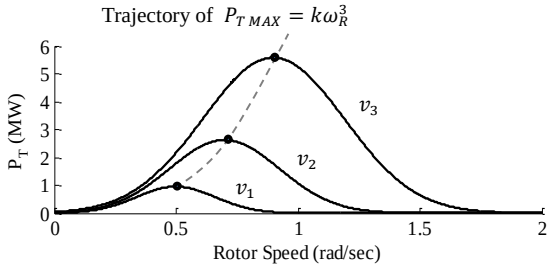

Fig. 1. Captured power curves versus the rotor speed, ω_R, for three wind speeds, $v_1 < v_2 < v_3$, and trajectory of the maximum power points.

Then, a second order sliding mode controller is designed to calculate the desired electrical torque such that the error approaches zero in a finite time. In this technique, the optimum value of the square-law gain is considered as a known parameter for a wind turbine.

Herein, the presented technique is a novel version of the conventional technique, i.e. $k\omega_R^2$, in which the proportional-coefficient is adaptively adjusted in real-time. The significance of the presented technique in comparison with the aforementioned methods is that neither a perturbation signal, a lookup table, nor a power measurement is required. Also, the maximum power capture coefficient and the optimum tip-speed ratio are not assumed as known parameters. The presented technique demonstrates appropriate dynamic performance in the presence of wind turbulence and sudden speed changes, while some of the existing techniques are validated only for slowly varying wind speed.

III. Wind Turbine Aerodynamics

Power captured by wind turbines fluctuates due to the inherent variable nature of the wind speed. In general, three regions of operation are known in wind turbines [2]. In Region I, the wind speed is below a minimum level for turbine operation and thus no power can be captured, see Fig. 2. In Region II, the wind speed is between the wind turbine cut-in and rated speeds, where the rotor speed can be controlled to capture the maximum power as the wind speed varies. In Region II, the blade pitch angle is typically held constant at the optimal value providing maximum aerodynamic torque. In Region III, the wind speed is above a maximum rated speed where no maximum power seeking is required so the goal is to

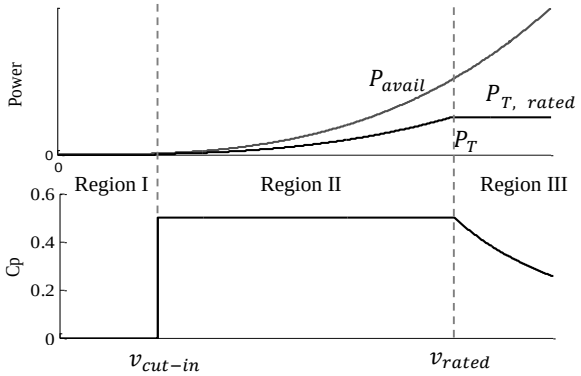

Fig. 2. Ideal available power, P_{avail}, captured power, P_T, and power capture coefficient, C_P, of a wind turbine in Regions I, II, and III.

2168-6777 (c) 2015 IEEE. Personal use is permitted, but republication/redistribution requires IEEE permission. See http://www.ieee.org/publications_standards/publications/rights/index.html for more information.

This article has been accepted for publication in a future issue of this journal, but has not been fully edited. Content may change prior to final publication. Citation information: DOI 10.1109/JESTPE.2015.2448633, IEEE Journal of Emerging and Selected Topics in Power Electronics

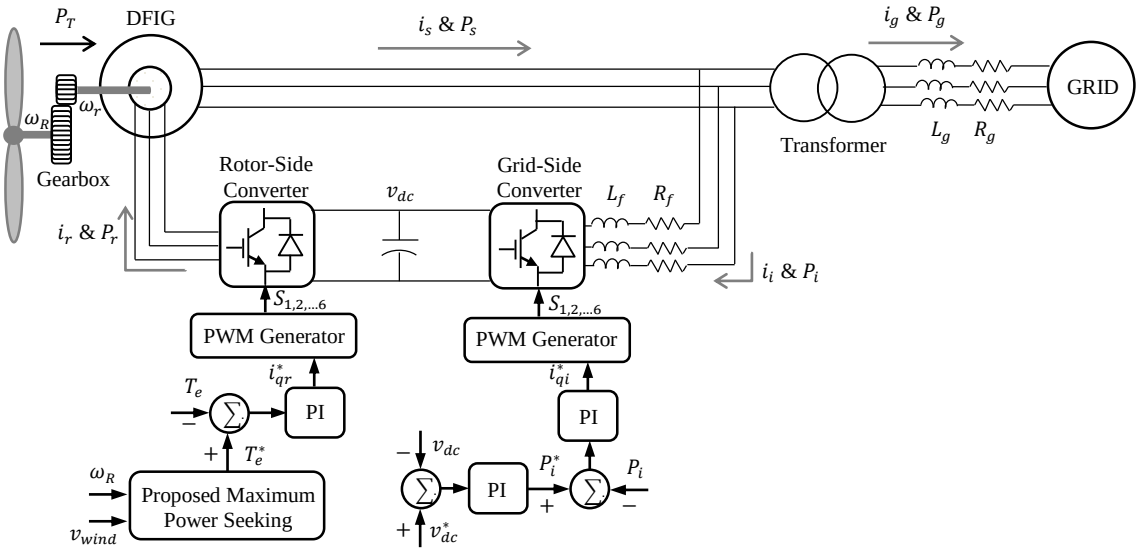

Fig. 3. Schematic of a DFIG based wind turbine system.

control the generator speed at its rated value by reducing extra aerodynamic power, which is done using blade pitch control.

Control in Region II is a complicated problem with nonlinear dynamics and immeasurable terms such as the rotor aerodynamic torque and the power capture coefficient. In the following, the wind turbine aerodynamic in Region II is briefly presented. The relationship between the mechanical input power and the wind speed normal to the turbine blades can be written in terms of available wind power, P_{avail}, as

$$P_{avail} = \frac{1}{2}\,\rho\, A\, v^3 \tag{1}$$

where ρ is the air density (1.225 kg/m3), A is the rotor swept area, and v is the wind speed. The power captured by the turbine, P_T, is a fraction of the available power expressed as

$$P_T = P_{avail}.\, C_p(\lambda, \beta) \tag{2}$$

where $C_p(\lambda, \beta)$ is the power capture coefficient, β is the blade pitch angle in rad, and λ is the dimensionless tip speed ratio given by

$$\lambda = \frac{\omega_R R}{v} \tag{3}$$

where ω_R is the rotor speed in rad/sec, and R is the blade radius in meter. Let T_{aero} denote the aerodynamic torque delivered to the turbine rotor, then the captured power is

$$P_T = T_{aero}\omega_R \tag{4}$$

Combining (1), (2), and (4) and then solving for T_{aero} (or mechanical torque, T_m) yields

$$T_{aero} = f(v, \omega_R) C_p(\lambda, \beta) \tag{5}$$

where $f = (1/2\omega_R)\rho A v^3$ for $\omega_R > 0$. Using the tip speed ratio in (3), one can show that T_{aero} is proportional to the square of the rotor speed. In addition to the wind turbine aerodynamic equations, the equation of motion for a coupled wind turbine and generator, referred to the rotor shaft, is

$$J\frac{d\omega_R}{dt} + C_D\omega_R = T_{aero} - T_e \tag{6}$$

where J is the equivalent lumped mass moment of inertia of the blades, rotor shaft, and drivetrain, C_D is the viscous friction coefficient of the drivetrain, and T_e is the electrical torque provided by the generator.

IV. Models of DFIG Wind Turbine Subsystems

The energy conversion in wind energy systems is achieved using two main devices. The first one is the extraction device, which harvests the mechanical power of the wind stream turning the wind turbine rotor, as briefly explained in the previous section. The other one is the generator which transforms the rotational mechanical power to electrical power [19]. Both permanent magnet synchronous generators (PMSG) and doubly fed induction generators (DFIG) are applied in wind energy conversion systems. Today, the DFIG is the most common type of generator in wind turbine systems. The DFIG is an induction machine with a wound rotor. In a DFIG-based wind turbine, the stator is directly connected to the grid while the rotor is connected through a back-to-back converter as shown in Fig. 3. The back-to-back converter needs only to handle the rotor power rating, which is about 30% of the nominal generator power. Therefore, there is a lower power loss in the converter of a DFIG compared to that in a PMSG where the converter handles the entire power. The overall system cost of a DFIG is also lower than a PMSG [20]. In the following subsection, the electrical model formulations of a DFIG-based wind turbine are presented. The electrical subsystem consists of a DFIG, power converters, filter, DC bus, and transmission line as shown in Fig. 3.

A. *DFIG model in $dq0$-reference frame*

If the stator and rotor variables are transformed into the rotating reference frame, the stator-rotor mutual inductances become independent of the high-speed rotor position, θ_r, and the rotor speed, ω_r. The $dq0$ (or Park's) transformation is used to convert the abc quantities to $dq0$ reference-frame—with a difference angle of θ between the frames, [21]. Hereafter, the subscripts d and q denote d- and q- axis

2168-6777 (c) 2015 IEEE. Personal use is permitted, but republication/redistribution requires IEEE permission. See http://www.ieee.org/publications_standards/publications/rights/index.html for more information.

This article has been accepted for publication in a future issue of this journal, but has not been fully edited. Content may change prior to final publication. Citation information: DOI 10.1109/JESTPE.2015.2448633, IEEE Journal of Emerging and Selected Topics in Power Electronics

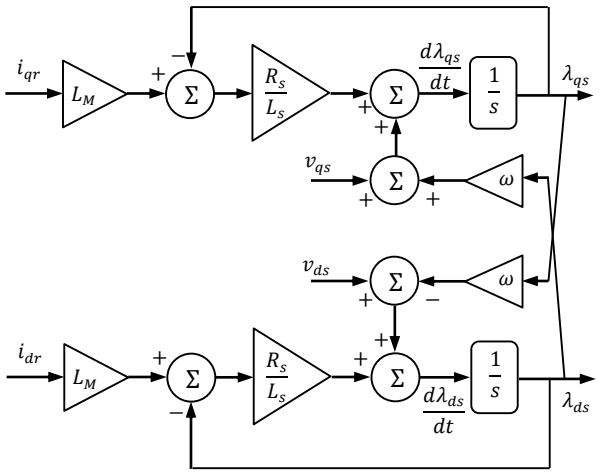

Fig. 4. Stator flux, λ_{qs} and λ_{ds}, calculations from the input signals, v_{qs} , i_{qr} , v_{ds} and i_{dr} .

quantities, e.g. for a voltage, v, a current, i, or a magnetic flux, λ. Also, the subscripts r and s denote rotor and stator quantities, respectively. The positive directions for the stator and rotor currents are assumed as shown in Fig. 3. Using KVL for the stator windings, and then applying the Park transformation, the differential equations for the stator windings [21] can be written as

$$v_{qs} = -R_s i_{qs} + \frac{d\lambda_{qs}}{dt} - \omega\lambda_{ds} \tag{7}$$

$$v_{ds} = -R_s i_{ds} + \frac{d\lambda_{ds}}{dt} + \omega\lambda_{qs} \tag{8}$$

where R_s is the stator winding resistance per phase and ω is the angular speed of the dq-reference frame. Fig. 4 shows these equations in block diagram form. The same calculation steps can be performed for the rotor circuits where, in the $dq0$ transformation for the rotor quantities, the θ term is replaced by $(\theta - \theta_r)$. This yields

$$v_{qr} = R_r i_{qr} + \frac{d\lambda_{qr}}{dt} + (\omega - \omega_r)\lambda_{dr} \tag{9}$$

$$v_{dr} = R_r i_{dr} + \frac{d\lambda_{dr}}{dt} - (\omega - \omega_r)\lambda_{qr}. \tag{10}$$

The stator flux linkage equations can also be converted to the $dq0$ reference frame as

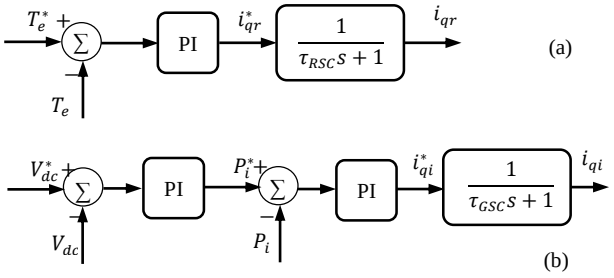

Fig. 5. (a) Rotor side converter, i_{dr} is set to zero and i_{qr} is controlled based on the desired generator torque, T_e^* (top), and (b) Grid side converter, i_{di} is set to zero and i_{qi} is controlled based on the desired DC-bus voltage, V_{dc}^* (bottom).

$$\lambda_{qs} = -L_s i_{qs} + L_M i_{qr} \tag{11}$$

$$\lambda_{ds} = -L_s i_{ds} + L_M i_{dr} \tag{12}$$

where L_M is the mutual-inductance and L_s is the stator self-inductance. Similarly, the rotor flux linkage equations can also be converted to the $dq0$ reference frame as

$$\lambda_{qr} = L_r i_{qr} - L_M i_{qs} \tag{13}$$

$$\lambda_{dr} = L_r i_{dr} - L_M i_{ds} \tag{14}$$

where L_r is the rotor self-inductance. Finally, the developed electromagnetic torque in a DFIG is obtained from

$$T_e = \left(\frac{3}{2}\right)\frac{p}{2}\left(\lambda_{ds} i_{qs} - \lambda_{qs} i_{ds}\right) \tag{15}$$

where p is the number of poles [21]. Eqs. (7) through (15) are all the equations needed to model a DFIG for this work. The stator voltages, v_{qs} and v_{ds}, are detected by the grid, and the rotor currents, i_{qr} and i_{dr}, are controlled by the rotor side converter, accordingly, λ_{qs} and λ_{ds} are obtained as shown in Fig. 4. Other quantities can be calculated using algebraic equations, e.g. i_{qs}, i_{ds}, from (9) and (10) (neglecting $d\lambda_{qr}/dt$ and $d\lambda_{dr}/dt$) and T_e from (15).

B. Rotor and Grid Side Converters

The solid-state based converters have much faster dynamics than the windmill and generator, therefore, to study the slow dynamic phenomena, the rotor- and stator-side converters can be modeled by their controllers and first-order transfer functions as shown in Fig. 5. In the rotor-side converter, i_{dr} is set to zero, and i_{qr} is controlled based on the desired electrical torque, T_e^*, as shown in Fig. 5(a). In the grid-side converter, both the DC-bus voltage and the power must be measured. However, the grid-side converter power can be calculated as

$$P_i = \frac{3}{2}\left(v_{qi} i_{qi} + v_{di} i_{di}\right) \tag{16}$$

where v_{qi} and v_{di} are the quadrature and direct inverter voltages, respectively, and are obtained from v_{qs} and v_{ds} as will be seen. The grid-side converter is connected to the stator and the grid through an RL circuit that is a simplified representation of a low-pass filter and the step-up transformer shown in Fig. 3. Using KVL equations and the dq0 transformation, v_{qi} and v_{di} are obtained from

$$v_{qi} = v_{qs} - R_f i_{qi} - L_f \frac{di_{qi}}{dt} - \omega L_f i_{di} \tag{17}$$

$$v_{di} = v_{ds} - R_f i_{di} - L_f \frac{di_{di}}{dt} + \omega L_f i_{qi}. \tag{18}$$

where v_{qs} and v_{ds} are obtained from a similar set of differential equations for the transmission line, assuming the grid voltage is known. Neglecting the converters' switching losses and using KCL, the DC-bus voltage is calculated as

$$\frac{1}{2C}\frac{d}{dt}(v_{dc})^2 = P_r - P_i \tag{19}$$

where, C is the DC-bus capacitor, P_r is the rotor side power, and P_i is the grid-side converter power as shown in Fig.3. In the back-to-back converter, the desired electrical torque identifies the desired value of i_{qr}, whereas for the rotor side converter the desired value of the DC-bus voltage identifies the desired value of active power in the grid-side converter

2168-6777 (c) 2015 IEEE. Personal use is permitted, but republication/redistribution requires IEEE permission. See http://www.ieee.org/publications_standards/publications/rights/index.html for more information.

This article has been accepted for publication in a future issue of this journal, but has not been fully edited. Content may change prior to final publication. Citation information: DOI 10.1109/JESTPE.2015.2448633, IEEE Journal of Emerging and Selected Topics in Power Electronics

and subsequently commands the desired value of i_{qi}. Both these converter models are illustrated in Fig. 5(a) and (b) respectively.

C. Model of Windmill Dynamics

The overall model for the validation of the proposed control scheme includes the entire windmill from wind to grid. Therefore, the FAST simulator is used in the MATLAB/Simulink environment along with the DFIG and converter models discussed earlier. The FAST simulator includes the aerodynamics and mechanical aspects of the wind turbine. FAST reads mechanical and aerodynamic system parameters from input files and creates dozens of mechanical output files to exchange with the Simulink model [18], [22]. In this work, the key inputs to FAST are the wind speed profile and electrical torque, and the main outputs are mechanical (aerodynamic) torque, T_{aero}, and low-speed rotor speed, ω_R. The electrical parts and controller, implemented by Simulink blocks, are coupled to the output of the FAST simulator. The NREL 5MW reference turbine [23], a test model for many studies, e.g. in [10], [13], and [14], is used to connect to the electrical and control subsystems developed in this work.

V. Proposed Control Schemes for Maximum Power Seeking in Wind Turbines

In the proposed technique, three control loops/laws are implemented to (i) determine the desired electrical/generator torque, T_e^*, in the DFIG, (ii) estimate the wind turbine power capture coefficient, $\hat{C}_P$, and (iii) calculate the desired rotor speed, ω_R^*, at which the wind turbine captures the maximum available wind power, as shown in Fig. 6. These control laws are elaborated in the following subsections.

A. Feedback Linearization for the Torque Control

The idea of feedback linearization is to implement a feedback loop in order to transform the nonlinear system into an equivalent linear one by changing the control input signal. This technique is different from conventional linearization (i.e. Jacobian linearization) [24]. As discussed earlier in Section III, the aerodynamic or mechanical torque is the nonlinear term of the equation of motion in (6). If the aerodynamic torque in (5) can be estimated, then, the nonlinearity of the equation of motion can be cancelled using the following control law

$$T_e^* = \hat{C}_p f(v, \omega_R) - u(t) \tag{20}$$

where $\hat{C}_p$ is the estimated value of the power capture coefficient and $f(v, \omega_R) = (\rho A v^3 / 2\omega_R) \propto \omega_R^2$ as defined in (5). The strategy is to make T_e follows the desired value, T_e^*, which results in a linear input-output dynamic behavior for the equation of motion, i.e. $J\dot{\omega}_R + C_D\omega_R = u(t)$. Therefore, the key is to estimate the power coefficient, which will be explained in the next subsection.

B. Lyapunov Approach for the Power Capture Coefficient Estimation

Estimation of the power capture coefficient, C_p, is used herein for maximizing power capturing. Although from (4) or (5), the C_p value can theoretically be calculated through rotor torque measurement, the common approach is to estimate the torque indirectly. In this work, the estimation of C_p is achieved using a Lyapunov-based analysis. The candidate Lyapunov function, $V \geq 0$, is chosen as

$$V = \frac{1}{2}J\tilde{\omega}_R^2 + \frac{1}{2}\gamma\tilde{C}_p^2 \tag{21}$$

where γ is a constant to be determined, $\tilde{\omega}_R = \omega_R^* - \omega_R - \varepsilon$ for $0 < \varepsilon \ll 1$, and $\tilde{C}_p = C_p^* - \hat{C}_p \geq 0$, in which C_p^* is a constant greater than the maximum accessible value of C_p, e.g. one can choose $C_p^* = 1$. Computing the time derivative of (21) yields

$$\dot{V} = J\tilde{\omega}_R\dot{\tilde{\omega}}_R + \gamma\tilde{C}_p\dot{\tilde{C}}_p. \tag{22}$$

Neglecting the viscous damping torque, $C_D\omega_R$, of the overall system, applying $\dot{\tilde{\omega}}_R = \dot{\omega}_R^* - \dot{\omega}_R$ and substituting $\dot{\omega}_R$ from (6) into (22) yields

$$\dot{V} = J\tilde{\omega}_R\dot{\omega}_R^* - \tilde{\omega}_R\left(C_p f - \hat{C}_p f + u\right) + \gamma\tilde{C}_p\dot{\tilde{C}}_p. \tag{23}$$

Substituting for $\tilde{C}_p$ into (23), yields

$$\dot{V} = J\tilde{\omega}_R\dot{\omega}_R^* - \tilde{\omega}_R\left(C_p f - \hat{C}_p f + u\right) - \gamma\dot{\hat{C}}_p\left(C_p^* - \hat{C}_p\right). \tag{24}$$

This last result can be rewritten as

$$\dot{V} = \hat{C}_p\left(\tilde{\omega}_R f + \gamma\dot{\hat{C}}_p\right) - \tilde{\omega}_R u + J\tilde{\omega}_R\dot{\omega}_R^* - C_p f\tilde{\omega}_R - \gamma C_p^*\dot{\hat{C}}_p. \tag{25}$$

The strategy is to make $\dot{V}$ a non-positive quantity. The first term in (25) is chosen to be zero, i.e.

$$\hat{C}_p\left(\tilde{\omega}_R f + \gamma\dot{\hat{C}}_p\right) = 0. \tag{26}$$

Herein, $\hat{C}_p$ is not always equal to zero, therefore the term in the parenthesis must be zero, resulting in the differential equation

$$\dot{\hat{C}}_p = -\frac{1}{\gamma}\tilde{\omega}_R f(v, \omega_R). \tag{27}$$

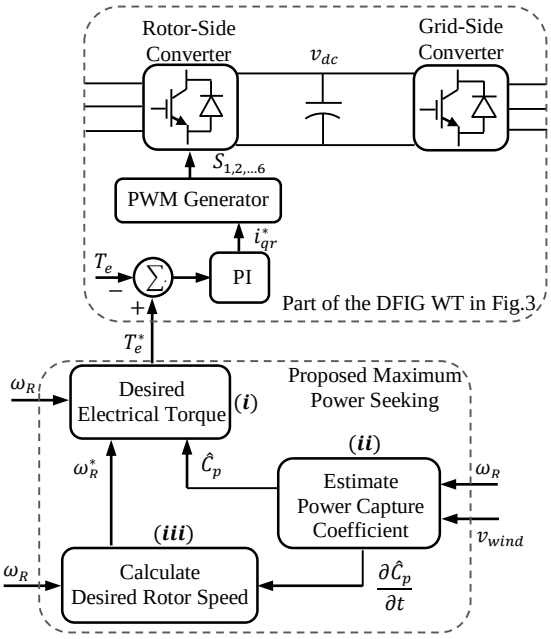

Fig. 6. Block diagram of the proposed control scheme for maximum power seeking in DFIG-based wind turbines that includes (*i*) the desired electrical torque calculator, (*ii*) wind turbine power capture coefficient, $\hat{C}_p$, estimator, and (*iii*) a desired rotor speed, ω_R^*, calculator.

2168-6777 (c) 2015 IEEE. Personal use is permitted, but republication/redistribution requires IEEE permission. See http://www.ieee.org/publications_standards/publications/rights/index.html for more information.

This article has been accepted for publication in a future issue of this journal, but has not been fully edited. Content may change prior to final publication. Citation information: DOI 10.1109/JESTPE.2015.2448633, IEEE Journal of Emerging and Selected Topics in Power Electronics

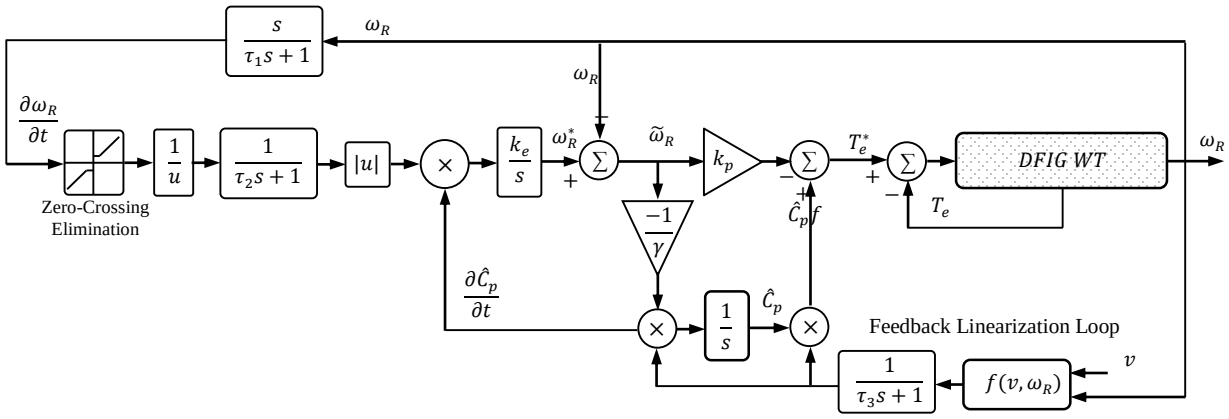

Fig. 7. The detailed control loops of the proposed maximum power seeking block.

the solution of which provides the estimated power capture coefficient, see Fig. 7. Now, to keep the second term on the right in (25), a non-positive value, the control input can be chosen as $u(t) = k_p\widetilde{\omega}_R$. Therefore, (20) can be rewritten as

$$T_e^* = -\frac{1}{\gamma} f(v,\omega_R) \int \widetilde{\omega}_R f(v,\omega_R) dt - k_p \widetilde{\omega}_R \qquad (28)$$

The torque control scheme including the feedback linearization loop and the power capture coefficient estimation is shown in Fig. 7. Substituting (26), $u(t) = k_p\widetilde{\omega}_R$, and (27) in (25) yields

$$\dot{V} = -k_p\widetilde{\omega}_R^2 + J\widetilde{\omega}_R\dot{\omega}_R^* + \left(C_p^* - C_p\right)\widetilde{\omega}_R f \qquad (29)$$

In the following subsection, $\dot{\omega}_R^*$ is identified to keep (29) always a non-positive value, $\dot{V} \le 0$.

C. Extremum Power Seeking Strategy

In order to hold $\dot{V} \le 0$, examining (29), one can choose $\dot{\omega}_R^* \propto (-\widetilde{\omega}_R)$, and select k_p adequately large that the first term holds a sufficiently large negative value with respect to the third term in (29). Recall that $\dot{\hat{C}}_p \propto (-\widetilde{\omega}_R)$, so one can choose

$$\dot{\omega}_R^* = k\dot{\hat{C}}_p. \qquad (30)$$

TABLE I
ELECTRICAL PARAMETERS

Parameter	Unit	Value
Generator No. of Poles, p	--	6
Generator Stator Rated Voltage	kV	3.75
Stator Resistance, R_s	mΩ	30.7
Rotor Resistance, R_r	mΩ	40.3
Stator Leakage Inductance, L_{ls}	mH	0.49
Rotor Leakage Inductance, L_{lr}	mH	0.59
Magnetizing Inductance, L_M	mH	44.5
DC-bus Rated Voltage	kV	4.00
DC-bus Capacitor, C	μF	8000
Converter Filter Resistance, R_f	mΩ	10
Converter Filter Inductance, L_f	mH	0.5
Transformer Ratio	--	1:10
Transmission Line Resistance, R_g	mΩ	10
Transmission Line Inductance, L_g	mH	100

This is consistent with the fact that the maximum value of $C_p = P_T/P_{avail}$ and captured power, P_T, for a constant wind speed occurs at the same point at which $\partial P_T/\partial\omega_R = 0$, as shown in Fig. 1. In the hill-climbing and perturb-and-observe techniques, the maximum power is sought according to the sign of $\partial P_T/\partial\omega_R$ such that if the wind turbine operating point is on the left side of the maximum point of the power curve, the desired rotor speed must be increased and if it is on the right side of the maximum point, then the rotor speed must be decreased. The forgoing discussion is valid for a constant or a slowly varying wind speed case. However, if the wind speed suddenly changes, two scenarios are possible:

i. Wind speed increases and thus, $\dot{\omega}_R > 0$ and $\dot{P}_T > 0$, or
ii. Wind speed decreases and thus, $\dot{\omega}_R < 0$ and $\dot{P}_T < 0$.

Using the chain rule, it can be concluded that for both the scenarios $(\partial P_T/\partial\omega_R) > 0$. This means that the hill-climbing and perturb-and-observe techniques can fail in case of a sudden wind speed change [16]. The same argument is true if the sign of $\partial C_p/\partial\omega_R$ is used. While C_p is not available, $\hat{C}_P$ and its derivative are available from in control scheme shown in Fig. 7. However, to prevent a mistake in maximum power seeking due to a sudden wind speed change, and according to (30), herein the proposed formula for $\dot{\omega}_R^*$ is given as follows:

$$\dot{\omega}_R^* = k_e \frac{\partial \hat{C}_P/\partial t}{|\partial\omega_R/\partial t|} \qquad (31)$$

where the denominator adaptively controls the rate of change in the desired rotor speed such that the gain in (30) is inversely updated based on the rotor speed acceleration. In practice, a zero-crossing elimination for the $|\partial\omega_R/\partial t|$ calculation is

TABLE II
CONTROL PARAMETERS USED IN THE SIMULATION

Parameter	Unit	Value
Coefficient (k_p) in Fig. 7	--	10^5 – 10^6
Coefficient (γ) in Fig. 8	--	10^6 – 10^7
Time Constant (τ_1) in Fig. 9	sec	0.1
Time Constant (τ_2) in Fig. 9	sec	4
Time Constant (τ_3) in Fig. 9	sec	2
Coefficient (k_e) in Fig. 9	--	$0.002 - 0.02$

2168-6777 (c) 2015 IEEE. Personal use is permitted, but republication/redistribution requires IEEE permission. See http://www.ieee.org/publications_standards/publications/rights/index.html for more information.

This article has been accepted for publication in a future issue of this journal, but has not been fully edited. Content may change prior to final publication. Citation information: DOI 10.1109/JESTPE.2015.2448633, IEEE Journal of Emerging and Selected Topics in Power Electronics

needed to prevent any potential numerical problem, as shown in Fig. 7. In this figure, the first transfer function is designed to obtain the time derivative of the angular speed, ω_R. Accordingly, τ_1 and τ_2 are chosen such that slow dynamics of the mechanical system can be observed, while measurement noises and spikes due to numerical calculation are effectively filtered.

The proposed extremum seeking technique captures the maximum power while the dither/perturbation signal is not needed and it does not fail in case of a sudden wind speed change. It should be noted that the wind speed profile must be sufficiently rich, as defined in [25], in order to achieve the best results. Also, the experience gained in tuning the control system demonstrated that the constant k_e in (31) and the constant γ in (27) play the greatest influence in achieving the power capture peak by either slowing or hastening the attainment of the proper value of ω_R^* for a given wind speed. The constant γ can be chosen as a value below the wind turbine inertia.

VI. Verification of the Proposed Control Scheme

In order to investigate the performance of the proposed control scheme, the system shown in Fig. 3 has entirely been modeled in the MATLAB/Smiulink environment. The model consists of the NREL 5 MW reference turbine simulator connected to a DFIG through a gearbox with a 1:97 ratio, along with power converters and transmission line. The electrical parameters are given in Table I. The control system has also been developed in the Matlab/Simulink environment, and the control parameters are given in Table II. Two wind speed profiles (including sudden wind speed step changes and wind turbulence) in the region II of the 5MW wind turbine have been used to investigate the validity of the proposed technique and the results are presented in this section. In these tests, the control parameters, γ and k_p, were set to be equal to 2×10^6 and 0.1×10^6, respectively, and k_e was defined as a function of the wind speed in Region II. However, a much larger value for k_e, e.g. $k_e = 1$, would be used in Region I, i.e. when $v < 5$ m/sec or $\omega_R < 7.2$ rad/sec for the 5MW wind turbine.

In the first case study, the wind speed is set to contain two step changes, the first one is from 8 m/sec to 7 m/sec at $t = 800$ sec, and the second change is from 7 m/sec to 9 m/sec at $t = 1400$ sec. In Fig. 8(a)-(d), the wind speed, desired and actual rotor speed, aerodynamic and desired electrical torque,

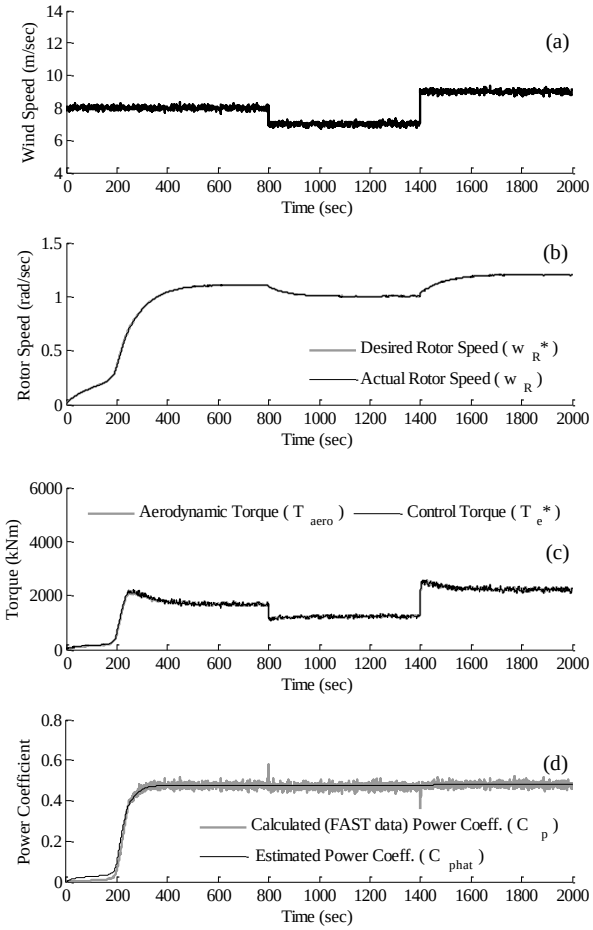

Fig. 8. The system response to the wind speed changes (a) Wind speed in m/sec (b) Actual, ω_R, and desired, ω_R^*, rotor speed in rad/sec, (c) Aerodynamic torque and control torque in kNm, and (d) Actual and estimated power coefficient— $\hat{C}_p$ reached its extremum value.

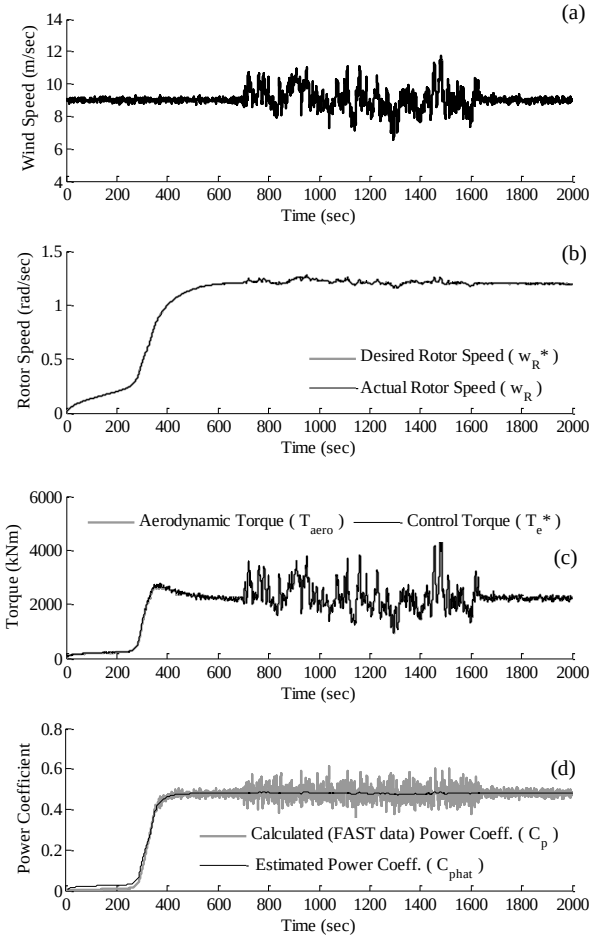

Fig. 9. The system response to a wind speed turbulence occurs between t =700 and 1650 sec, (a) Wind speed profile in m/sec, (b) Actual and desired rotor speed in rad/sec, (c) Aerodynamic torque and control torque in kNm, and (d) Actual and estimated power coefficient— $\hat{C}_p$ holds its extremum value.

2168-6777 (c) 2015 IEEE. Personal use is permitted, but republication/redistribution requires IEEE permission. See http://www.ieee.org/publications_standards/publications/rights/index.html for more information.

This article has been accepted for publication in a future issue of this journal, but has not been fully edited. Content may change prior to final publication. Citation information: DOI 10.1109/JESTPE.2015.2448633, IEEE Journal of Emerging and Selected Topics in Power Electronics

and finally the actual and estimated power capture coefficient are shown, respectively. Fig. 8(b) shows that the actual rotor speed closely follows the desired rotor speed that is calculated from the extremum seeking control scheme given in (31). The speed regulation is such that it is difficult to discern any difference between the desired rotor speed and the actual rotor speed. Fig. 8(c) shows that the aerodynamic torque also follows the control torque obtained from (28). As shown in Fig. 8(d), the actual power capture coefficient (calculated from the FAST wind turbine simulator output data) and the estimated $\hat{C}_P$ reside around the maximum value of 0.48 for the 5MW wind turbine. Notice that the desired rotor speed is adjusted in response to the wind speed step changes to hold the maximum power capture coefficient.

In the second case, the system response to real wind turbulence occurring between $t = 700$ sec and $t = 1650$ sec is investigated. For $0 < t < 700$ and $t > 1650$, the average wind speed value was set to 9 m/sec. Fig. 9(a) illustrates the wind speed profile, and Fig. 9(b) shows the desired rotor speed and its actual value. As can be seen, rotor speed follows the desired speed. The desired rotor speed, ω_R^*, in Figs. 6 and 7 is controlled to track the maximum available power and the actual rotor speed closely follows it during the wind speed turbulence. In Fig. 9(c), the aerodynamic torque and the control law torque given by (28) are shown for this case study. As shown, the generator torque follows the aerodynamic torque. From the results shown in Figs. 8 and 9, it can be seen that the calculated desired speed is adjusted automatically to keep $\hat{C}_P$ at its maximum value, herein 0.48 p.u. Thus, the desired rotor speed changes and tracks the desired value. It can also be observed that the controller works in different wind speed conditions so that the estimated power capture coefficient is maintained at its maximum value, even in the event of sudden step changes and turbulence in the wind speed. From the estimated power capture coefficients shown in Figs. 8(d) and 9(d), it can be seen that regardless of the wind speed profiles, the estimated power coefficient attempts to stay near the extremum value.

VII. Analysis and Discussions

In this section, three different features of the proposed control scheme are examined; (i) the sensitivity of the control parameters, (ii) the flexibility to adapt the blade pitch controller in Region III, and (iii) the dynamic response in Region II. In the first subsection, sensitivity of the proposed control scheme for maximum power seeking is studied in terms of variations of two main control parameters for different wind speeds. Second, dynamic behavior of the control scheme is shown when the pitch control scheme is activated to keep the power and rotor speed in their rated values in Region III. In the third subsection, a comparison study between the proposed adaptive control scheme and the conventional technique, i.e. the electrical torque is proportional to the square of the rotor speed as given by $k\omega^2$, is presented through simulation results.

A. Sensitivity Analysis of the Control Parameters:

For this study, the two main control parameters in (28), i.e. k_p and γ were changed within their acceptable limits and the power capture coefficient, C_p was measured for the case study 5MW wind turbine. The outcomes of this study are shown in Fig. 10(a) and (b), respectively. In Fig. 10(a), C_p varies between 0.4829 and 0.4059 for a wide range of γ and three different wind speeds, i.e. $v = 7$, 8, and 9 m/s in Region II. Also, in Fig. 10(b), C_p varies between 0.4840 and 0.4563 for the wind speed and different k_p values. As can be seen, the control scheme is more sensitive to γ than k_p. Notice, C_p remains above the acceptable value of 0.477, and values of $\partial C_p/\partial\gamma$ and $\partial C_p/\partial k_p$ are insignificant for $10^5 \le k_p \le 10^6$ and $10^6 \le \gamma \le 10^7$. In addition to the results shown in the previous section for different wind speed profiles, these plots confirm that the maximum power seeking can successfully be achieved over relatively wide ranges of variations of the control parameters, but the best result occurs at $\gamma \cong 2 \times 10^6$ and $k_p = 0.1 \times 10^6$.

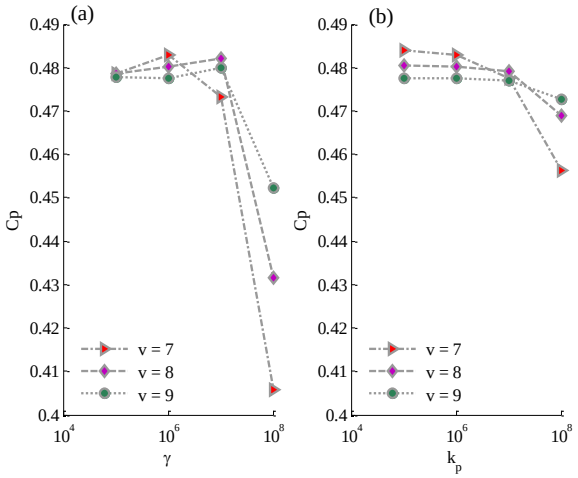

Fig. 10. The control scheme sensitivity to control parameters for three different wind speed values, plot of (a) C_p versus γ for $k_p = 10^6$, and (b) $C_p$versus k_p for $\gamma = 10^6$.

B. Transition between Region II and Region III:

A technical challenge for any maximum power seeking scheme for wind turbines is to provide seamless transitions between Regions II and III. Notice that the maximum power seeking is only performed in Region II and the blade pitch control is activated to keep the rotor speed and power at their rated values in Region III. The control strategy in Region III is to regulate the generator torque at its maximum value, i.e. $P_{rated}/\omega_{R\,max}$ (at the low-speed shaft). Consequently, as the wind speed increases in Region III, the accelerating torque, i.e. $T_{aero} - T_e$, increases, and thus, the rotor speed increases. However, an increase in blade pitch angle can reduce T_{aero} . Hence, the rotor speed can be controlled at its rated value, i.e. $\omega_{R\,max}$ and the output power remains at its rated value. Moreover, in the proposed control scheme, for a seamless transition between the regions, f in (28) can be defined as

$$f = \begin{cases} \dfrac{1}{2}\dfrac{\rho A v^3}{\omega_{R\,min}}, & 0 \le \omega_R < \omega_{R\,min} \quad I \\ \dfrac{1}{2}\dfrac{\rho A v^3}{\omega_R}, & \omega_{R\,min} \le \omega_R < \omega_{R\,max} \quad II \\ \dfrac{P_{rated}}{\omega_{R\,max} C_{p\,max}}, & \omega_R \ge \omega_{R\,max} \quad III \end{cases} \tag{32}$$

2168-6777 (c) 2015 IEEE. Personal use is permitted, but republication/redistribution requires IEEE permission. See http://www.ieee.org/publications_standards/publications/rights/index.html for more information.

This article has been accepted for publication in a future issue of this journal, but has not been fully edited. Content may change prior to final publication. Citation information: DOI 10.1109/JESTPE.2015.2448633, IEEE Journal of Emerging and Selected Topics in Power Electronics

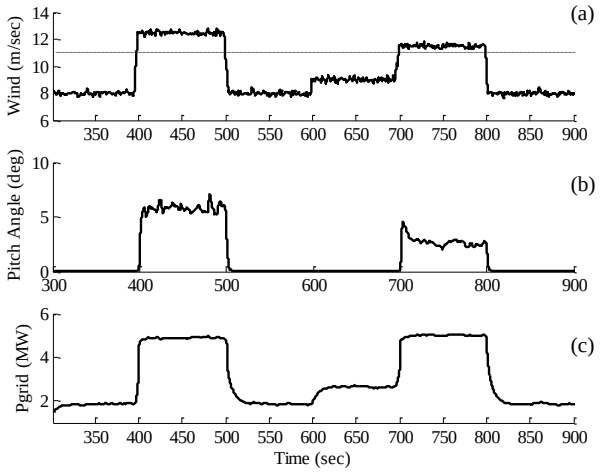

Fig. 11. The system response to a wind speed profile with the wind speeds above 11 m/sec (Region III) (a) Wind speed in m/sec (b) Blade pitch angle in degrees, and (c) Power injected to the power grid in MW.

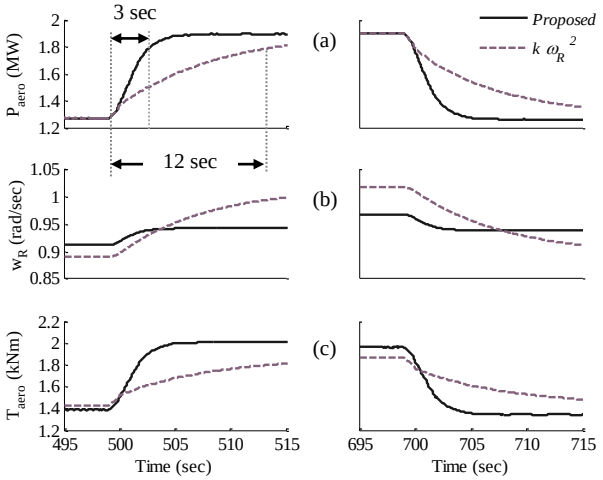

Fig. 12. The system responses (solid-lines indicate the results of the proposed method, and the dash-lines indicate the results of the conventional method) to two step changes in wind speed profile (7 to 8 m/sec at t=499sec, and 8 to 7 m/sec at t=699 sec) (a) Rotor speed in rad/sec (b) Mechanical (aerodynamic) torque in kNm, and (c) Power injected to the power grid in MW.

where, $\omega_{R\,min}$ and $\omega_{R\,max}$ are the rated minimum and maximum rotor speed values. Also, a region called Region 2.5 can be implemented into the proposed scheme to further smooth the transition between Region II and III. Also, the calculated f should be passed through a first-order low-pass filter to avoid any sudden change in (28) caused by wind speed variations or transitions between the regions. In the proposed controller, a compensator torque command signal is fed to the generator to suppress the rotor speed overshoot during the Region II to III transient. In Fig. 11, the wind speed, the power injected into the grid, and blade pitch angles are shown. As can be seen in this figure, the controller can effectively clamp the output power at 5MW when the wind speed goes above 11 m/s, i.e. Region III.

C. *A Comparison between $k\omega^2$ and the Proposed Control Scheme:*

A comparison between desired (control) torque equation in the conventional method, i.e. $T_e^* = k_{opt}\omega^2$, and in the proposed method, eq. (28), substituting $v = \omega_R R/\lambda_{opt}$ shows the similarity between the two methods. Despite the disadvantages of the conventional method mentioned in the literature, e.g. in [2] and [10], the ease of implementation is the key advantage. However, dynamic behaviors of the two methods are different as three control parameters, i.e. k_e, γ and k_p, exist in the proposed method. This can provide the flexibility to obtain the maximum C_p, while the rotor speed change at the event of a sudden change in the wind speed is smaller than that of $k\omega_R^2$. The small change in the rotor speed will reduce the amount of mechanical stresses on the drivetrain parts, i.e. gearbox, shaft, and blades. Accordingly, the lifetime of the wind turbine can be improved. In order to demonstrate this difference the results obtained from both methods are compared in Fig. 12. Notice that k_{opt} is set to 1.8×10^6 for the case study 5MW DFIG-based wind turbine to obtain $C_p = 0.48$. The power capture, rotor speed, and mechanical torque are shown in Fig. 12. The only difference between the simulated systems was the controller or command torque signal, i.e. T_e^*. In this figure, the wind speed has a step change at $t = 499\ sec$ from 7 to $8\ m/s$ and then back to 7 at $t = 699\ sec$. Notice that the rise-time response of the power in the proposed technique is about 3 seconds whereas in the conventional method the rise-time is about 12 seconds, as shown in Fig. 12. A comparison between these figures demonstrates that the dynamic response of the proposed controller is faster than the conventional, $k\omega^2$, controller, while the rotor speed variation due to a step change in the wind speed is small for the proposed controller.

VIII. Conclusion

In this paper, an adaptive nonlinear control scheme for DFIG-based wind turbines has been developed using a Lyapunov-based analysis and feedback linearization. The control scheme is built from three control laws to (i) determine the desired generator torque, (ii) estimate the wind turbine power capture coefficient, and (iii) calculate the desired rotor speed at which the wind turbine captures the maximum available wind power. The control scheme adaptively estimates the wind power capture coefficient using real-time wind and rotor speed values. This control system was developed in a MATLAB/ Simulink environment and the overall system was simulated using the NREL 5MW FAST reference turbine connected to a developed DFIG, back-to-back converters, and a transmission line between the DFIG and the power grid. The two main control schemes, i.e. power capture coefficient estimation with rotor speed regulation and desired rotor speed calculation based on maximizing the estimated power capture coefficient, have shown robust dynamic behaviors. The role of the controller is to adaptively reach the maximum power capture coefficient as the wind speed changes. The significance of the presented technique in comparison with the existing methods is that a perturbation signal is not required. Also, neither the maximum power capture coefficient, nor the optimum tip-speed ratio is assumed as a known parameter. Moreover, the presented technique demonstrates a robust dynamic performance in the

2168-6777 (c) 2015 IEEE. Personal use is permitted, but republication/redistribution requires IEEE permission. See http://www.ieee.org/publications_standards/publications/rights/index.html for more information.

This article has been accepted for publication in a future issue of this journal, but has not been fully edited. Content may change prior to final publication. Citation information: DOI 10.1109/JESTPE.2015.2448633, IEEE Journal of Emerging and Selected Topics in Power Electronics

presence of wind turbulence and sudden speed changes. The numerical results have demonstrated the validity and robustness of the developed control scheme.

ACKNOWLEDGEMENT

This work was supported in part by the industry sponsored KSU Electric Power Affiliates Program which the authors gratefully acknowledge.

REFERENCES

[1] W. E. Leithead and B. Connor, "Control of variable speed wind turbines: Design task," *Int. J. Control*, vol. 73, no. 13, pp. 1189–1212, 2000.

[2] K. E. Johnson, L. J. Fingersh, M. J. Balas, and L. Y. Pao, "Methods for increasing region II power capture on a variable-speed wind turbine," *Trans. ASME*, vol. 126, no. pp. 1092-1100, Nov. 2004.

[3] L.Y. Pao and K.E. Johnson, "A tutorial on the dynamics and control of wind turbines and wind farms" *in Proc. American Control conf.*, St. Louis, MO, June 10-12, 2009, pp. 2076 – 2089.

[4] T. Hawkins, W. N. White, G. Hu, F. D. Sahneh, "Region II wind power capture maximization using robust control and estimation with alternating gradient search," *in proc. American Control Conf.*, San Francisco, CA, June 29 - July 01, 2011, pp.2695-2700.

[5] A. Ghaffari, M. Kristic, and S. Seshagiri, "Power optimization and control in wind energy conversion systems using extremum seeking," *IEEE Trans. Energy Convers.*, vol. 22, no. 5, pp. 1684-1695, Sep. 2014.

[6] M.G. Simoes, B. K. Bose, and R. J. Spiegel, "Fuzzy logic based intelligent control of a variable speed cage machine wind generation system," *IEEE Trans. Power Electron*., vol. 12, no.1, pp. 87-95, 1997.

[7] R. Chedid, S. Karaki, and C. El-Chamali, "Adaptive fuzzy control for wind-diesel weak power systems," *IEEE Trans. Energy Convers*., vol.15, no.1, pp. 71–78, 2000.

[8] Hui Li, K.L. Shi, and P. McLaren, "Neural network based sensorless maximum wind energy capture with compensated power coefficient," *IEEE Trans. Ind. Appl*., vol. 41, no. 6, pp. 2600-2608, Nov./Dec. 2005.

[9] M. Pucci, and M. Cirrincione, "Neural MPPT control of wind generators with induction machines without speed sensors," *IEEE Trans. Ind. Electron*., vol. 58, pp. 37-47, 2011.

[10] E. Iyasere, M. Salah, D. Dawson, J. Wagner, and E. Tatlicioglu, "Optimum seeking-based non-linear controller to maximise energy capture in a variable speed wind turbine," *IET Control Theory & Appl.*, vol. 6, no. 4, pp. 526–532, 2012.

[11] J. H. Laks, L. Y. Pao, and A. D. Wright, "Control of Wind Turbines: Past, Present, and Future," *in Proc. American Control Conf*. St. Louis, MO, June 10-12, 2009, pp. 2096-2104.

[12] Q. Chen, Y. Li, Z. Yang, J. Seem, and J. Creaby, "Self-optimizing-robust control of wind power generation with doubly-fed induction generator," *in Proc. IEEE Conf. Dyn. Sys. & Control*, Cambridge, MA, Sep. 2010, pp.929-936.

[13] B. Boukhezzar and H. Siguerdidjane, "Nonlinear control of a variable-speed wind turbine using a two-mass model," *IEEE Trans. Energy Convers*., vol. 26, no. 1, pp. 149–162, 2011.

[14] B. Beltran, T. Ahmed-Ali, and M. Benbouzid, "High order sliding – mode control of variable-speed wind turbines," *IEEE Trans. Ind. Electron*., vol. 26, pp.149-162, 2009.

[15] L. D. Guerra, F. D. Adegas, J. Stoustrup and M. Monros, "Adaptive control algorithm for improving power capture of wind turbines in turbulent winds," *in Proc. American Control Conf.*, June 2012, pp. 5807 – 5812.

[16] SMR. Kazmi, H. Goto, G. Hai-Jiao, O. Ichinokura, "A novel algorithm for fast and efficient speed-sensorless maximum power point tracking in wind energy conversion systems," *IEEE Trans. Ind. Electron.*, vol. 58, pp. 29-36, 2011.

[17] F. Fateh, W. White, and D. Gruenbacher, "A nonlinear control scheme for extremum power seeking in wind turbine energy conversion systems," *in Proc. American Control Conf*., June 2014, pp. 1180 – 1185.

[18] J.M. Jonkman, and M.L. Buhl Jr., "FAST User's Guide, NREL/EL-500-29798," Golden, Colorado: *National Renewable Energy Laboratory*, 2005.

[19] L. Yazhou, A. Mullane, G. Ightbody, and R. Yacamini, "Modeling of the wind turbine with a doubly fed induction generator for grid integration studies," *IEEE Trans. Energy Convers.*, vol. 21, no. 1, pp. 257–264, Mar. 2006.

[20] A Peterson, T. Thiringer, and L. Harnefors, "Modeling and experimental verification of grid interaction of a DFIG wind turbine," *IEEE Trans. Energy convers.*, vol. 20, no. 4, pp. 878-886, Dec. 2005.

[21] D. W. Novotny, and T. A. Lipo, "Vector control and dynamics of AC drives," *Clarendon press Oxford*, 1996.

[22] G. Bir and J. Jonkman, "Aeroelastic instabilities of large offshore and onshore wind turbines," *J. Phys. Conf. Ser*. 75, 2007.

[23] J. Jonkman, S. Butterfield, W. Musial, and G. Scott, "Definition of a 5-MW reference wind turbine for offshore system development," Technical Report NREL/TP-500-38060, *National Renewable Energy Laboratory*, 2009.

[24] J.E. Slotine, and W. Li, "Applied nonlinear control," *Prentice Hall*, 1991.

[25] S. Boud, and S. Sastry, "On parameter convergence in adaptive control," Systems & Control Letters 3, pp. 311-319, Dec. 1989.

Fariba Fateh (S'11) received the M.Sc. degree in electrical engineering from Marquette University, Milwaukee, Wisconsin, USA, 2005. She is currently working toward the Ph.D. degree in electrical and computer engineering department at Kansas State University, Manhattan, KS, USA. Her research interests include system modeling, nonlinear control theory and control applications in wind turbines. She is a member of Phi kappa phi honor society.

Warren N. White received the B.Sc. degree in electrical engineering with honors from Tulane University, in 1974, the M.Sc. degree in electrical power engineering from Rensselaer Polytechnic Institute, in 1977, and the Ph.D. degree in mechanical engineering from Tulane University, in 1985. Since 1985, he has been with the mechanical and nuclear engineering department at Kansas State University, Manhattan, KS, USA. His main research interests consist of nonlinear control theory, underactuated mechanical systems, wind turbine control, power equipment rejected heat, and control education.

Don Gruenbacher (M'89) received the B.Sc. degree in 1989, the M.Sc. degree in 1991, and the Ph.D. degree in 1994, all in electrical engineering from Kansas State University.

He is currently serving as department head and associate professor in the Department of Electrical and Computer Engineering at Kansas State University. Prior to joining Kansas State University as a faculty member, he was a senior staff in the Space Department of the Johns Hopkins University Applied Physics Laboratory between 1994-1997 and 1989-1990. He has been recognized as an outstanding faculty member by both Eta Kappa Nu and Mortar Board. His research activities are focused in the areas of computer networks, communications, and digital design.

2168-6777 (c) 2015 IEEE. Personal use is permitted, but republication/redistribution requires IEEE permission. See http://www.ieee.org/publications_standards/publications/rights/index.html for more information.